Onset Mechanism for Granular Axial Band Formation in Rotating Tumblers

Pengfei Chen,[1] Julio M. Ottino,[1,2,3] and Richard M. Lueptow[2,*]

[1]*Department of Chemical and Biological Engineering, Northwestern University, Evanston, Illinois, 60208, USA*
[2]*Department of Mechanical Engineering, Northwestern University, Evanston, Illinois, 60208, USA*
[3]*The Northwestern Institute on Complex Systems (NICO), Northwestern University, Evanston, Illinois, 60208, USA*
(Received 27 October 2009; published 3 May 2010)

The mechanism for band formation of a granular mixture in long rotating tumblers is unresolved 70 years after the phenomenon was first observed. We explore the onset mechanism for axial segregation of a bidisperse mixture of particles of different sizes using the discrete element method. End walls initiate axial band formation via an axial flow due to friction at the end walls. The nonuniform distribution of axial velocity in the flow together with simultaneous radial segregation due to percolation result in small particles being driven further from the end walls, while larger particles accumulate at the end walls. Once this occurs, a cascading effect likely causes other bands to form due to the axial gradient in particle concentrations.

　　　　　　　　　　PACS numbers: 45.70.Mg, 45.70.Qj

A puzzling experimental result in granular flow is axial segregation of a bidisperse mixture of particles upon rotation in a partially filled long horizontal tumbler. Particles of two sizes segregate into bands rich in small or large particles over a large number, $O(100)$, of tumbler rotations. The phenomenon was first reported by Oyama [1], but did not attract much attention until recent decades [2–8]. Axial band formation is robust: it can occur in tumblers of square cross section [9], systems in which the interstitial fluid is a gas or a liquid [7], and in systems with a wide range of fill levels and rotational speeds [10,11]. Bands of large particles typically form first near the end walls of the tumbler [5,9,11] and eventually fill the tumbler. The bands are visible at the surface of the flowing layer and around the circumference of the tumbler, typically having a wavelength of about one tumbler diameter [11] before band coarsening. When observed using an interstitial fluid matched to the clear larger particles or using magnetic resonance imaging, what appears as a band of small particles is actually a region where the core of small particles reaches the surface. Bands of large particles are regions where an annulus of larger particles surrounds a small radius core of small particles [6,7,10].

The difference in the angle of repose for different particle types has been proposed as the origin of the bands [4–6,12]. Generally, the angle of repose of large particles is slightly steeper than that for small particles, and after the bands form, the concentration of large particles is in phase with the angle of repose along the length of the tumbler [13]. A proposed mechanism for band formation is based on the angle of repose for mixed large and small particles being larger than that for a region rich in large particles [6,12]. An initial fluctuation in particle concentration is assumed to result in a large-particle-rich region and mixed-particle region. As particles in a mixed phase region flow down the slope of the flowing layer, the smaller particles percolate to lower in the flowing layer leaving larger

particles to fall toward the adjacent large-particle-rich region, enhancing the initial fluctuation, eventually leading to bands.

Yet several questions remain unresolved. First, it has been observed that bulges in the axially segregated core of small particles may exist in the bulk without extending to the surface, so the axial segregation cannot be driven exclusively by the angles of repose at the surface [14]. Second, large-particle bands typically form first at the end walls of the tumbler [5,9,11] where the angle of repose is higher than in the bulk due to friction with the end wall. Third, if the angle of repose mechanism is correct, large particles would flow from the large-particle band (having a larger angle of repose) to the small-particle band (having a smaller angle of repose), but this does not occur. Finally, band merging occurs after many tumbler rotations via axial redistribution of small particles through the radial core, which cannot be explained by the angle of repose mechanism. Here we propose an alternative mechanism for the formation of bands based the radial segregation of particles of two sizes along with a small axial flow of particles in the flowing layer.

We use the discrete element method with an explicit, constant time step to integrate Newton's second law to describe the translational and rotational motion of individual ''soft'' particles in a tumbler. The linear-spring dashpot model [15–18] used to calculate the normal force between two contacting particles consists of two parts: a normal elastic spring force and a normal viscous damping force, $\mathbf{F}_{ij}^n = [k_n\alpha - 2\gamma_n m_{\mathrm{eff}}(\mathbf{V}_{ij}.\hat{\mathbf{r}}_{ij})]\hat{\mathbf{r}}_{ij}$. Here α and $\mathbf{V}_{ij}$ denote the particle overlap and relative velocity ($\mathbf{V}_i - \mathbf{V}_j$) of two contacting particles i and j. $\hat{\mathbf{r}}_{ij}$ is the unit vector between particles i and j, and $m_{\mathrm{eff}} = \frac{m_i m_j}{m_i+m_j}$ is the reduced mass of the two particles. k_n and γ_n characterize the stiffness and damping of the granular materials and are related to the collision time Δt and restitution coefficient e [16,18]. We use a tangential force model without a memory effect [19–

[22]: $\mathbf{F}_{ij}^t = -\min(|\gamma_s \mathbf{V}_{ij}^s|, |\mu \mathbf{F}_{ij}^n|)\,\mathrm{sgn}(\mathbf{V}_{ij}^s)$. $\mathbf{V}_{ij}^s$ is the relative tangential velocity of two particles, and γ_s is the tangential damping coefficient. The Verlet algorithm [16] is used to update the positions and velocities of particles.

The parameters of the simulations are as follows: the diameter of the tumbler is $D = 2R = 0.08$ m; the length of the tumbler is $L = 2D = 0.16$ m; equal volumes of small and large particles of radii 0.001 and 0.002 m fill 20% of the tumbler volume; gravitational acceleration is $g = 9.8$ m/s^2; particle properties correspond to glass (density $\rho = 2500$ kg/m^3, restitution coefficient $e = 0.97$ [16]). An initial random mixture of about 13 800 particles is simulated. To avoid a close-packed structure, the particles have a normal size distribution with a variance of $(0.1d)^2$, where d is the particle diameter. The friction coefficients between particles and between particles and walls are set to $\mu = 0.6$; in order to save computer time, the collision time is $\Delta t = 10^{-3}$ s, consistent with previous simulations [20] and sufficient for modeling hard spheres [23,24] based on similarity with preliminary results for $\Delta t = 10^{-4}$ s. The integration time step is $\Delta t/40 = 2.5 \times 10^{-5}$ s for numerical stability [16]. Except where noted, the rotational speed is $\Omega = 3.14$ rad/s. The curved cylindrical wall and two end walls of the tumbler are modeled as geometrically smooth surfaces, having infinite mass and radius. The origin of coordinate system is at the center of the tumbler with x along the streamwise direction, y normal to the free surface, and z along the tumbler axis. The surface of the flowing layer should be at $y = -0.0195$ m if the surface is perfectly flat and there is no dilation during flow.

The left-hand side of Fig. 1 shows the evolution of the volume concentration profile for small particles, $\langle C_s \rangle$, and large particles, $\langle C_l \rangle$, along the axis of rotation z, where $\langle\rangle$ denotes the cross-sectionally averaged values over one rotation. The concentrations deviate from the initially well-mixed state very quickly as large particles accumulate near the end walls within one rotation. After several rotations concentration bands appear near the end walls ($z = \pm 0.08$ m), consistent with experimental observations [5,9,11] that large-particle-rich bands appear near the end walls first. Adjacent bands rich in small particles also appear. After 20 rotations, axial segregation is evident along the entire length of the tumbler with a third band of large particles appearing at the axial center of the tumbler ($z = 0$). The concentrations reach a "steady" segregated state within 50 rotations, though the positions and concentrations of bands randomly fluctuate very slightly with time. The angle of repose in the center large-particle band is about 29° compared to about 27° in the small-particle bands. No merging of bands was evident up to 200 rotations in these simulations, which is not surprising given that this is a relatively short tumbler and that band merging typically occurs in experiments after $O(100)$ rotations and sometimes even much later [11].

Stream traces based on the streamwise (u) and axial (w) velocities on the surface of the flowing layer for the mix-
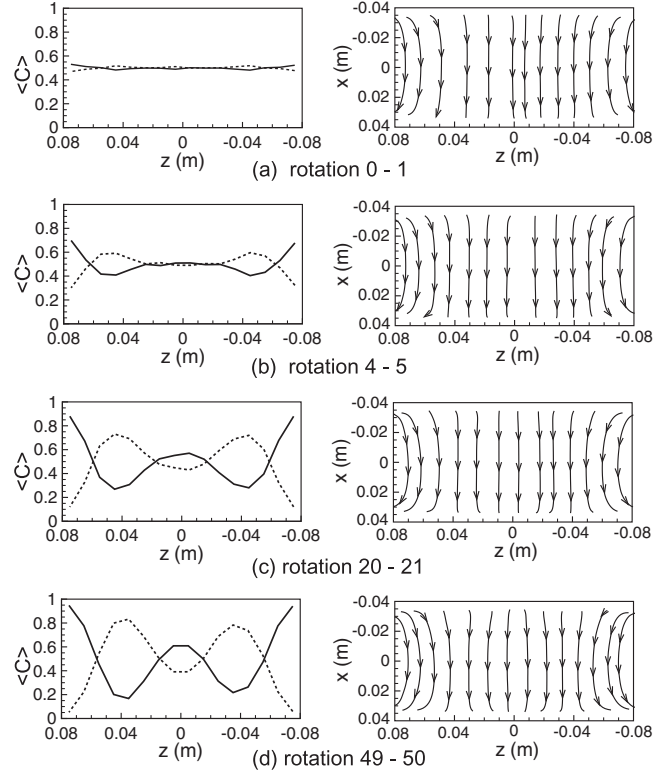

FIG. 1. Evolution of the cross-sectionally averaged species concentrations (left-hand column) and the stream traces on the free surface at $y = -0.02$ m (right-hand column) along the axial length at different times: (a) initial segregation (rotation 0–1); (b) intermediate segregation (rotation 4–5); (c) further segregation (rotation 20–21); (d) full segregation (rotation 49–50). Dashed lines, concentration of small particles $\langle C_s \rangle$; solid lines, concentration of large particles $\langle C_l \rangle$.

ture (both particle species) are shown on the right-hand side of Fig. 1. As axial segregation begins, the axial flow field at the free surface of the bidisperse system is similar to that for a monodisperse system; particles near the end walls move away from the end wall in the upstream portion of the flowing layer and then move back in the downstream portion due to mass conservation [18,25]. Streamwise flow of particles in the transverse slices nearest the end walls is slowed by the frictional end walls. Thus, the only way to conserve mass while accommodating the reduced streamwise velocity and the thinner flowing layer [18] near the end walls is for these particles to flow axially away from the end wall in the upper portion of the flowing layer and then back toward the end wall in the downstream portion.

As the segregation proceeds with the development of the two bands of small particles and the band of large particles at the center of the tumbler (at rotation 20–21), other axial flows appear. Particles in the center band flow toward the adjacent bands of small particles in the upstream portion of the flowing layer and back in the downstream portion. As axial segregation continues, these axial flows grow stronger. At steady state, particles in all three large-particle bands ($z = 0, \pm 0.08$ m) flow toward the adjacent bands of

small particles in the upstream portion of the flowing layer and back into the large-particle bands in the downstream portion. The magnitude of the axial velocity is negligible at the centers of the bands ($z = 0, \pm 0.04$ m). The maximum axial flows occur at the interface between bands (around $z = \pm 0.02, \pm 0.065$ m). Furthermore, the end-wall-related axial flow increases as the bands near the end walls develop.

The axial velocities of the two species are nearly identical during the entire course of axial segregation, consistent with previous results for radial segregation [20]. However, it is useful to consider how the axial flow and particle number densities combine to bring about the axial banding. Figure 2 shows the axial velocity of the mixture w as well as the number density n and axial particle flux q (particles/m^2 s), of both small and large particles averaged over rotation 0–1 on the same cross section, $z = 0.065$ m. The axial velocity of the mixture shown in Fig. 2(a) is almost symmetric about the midpoint of the flowing layer ($x = 0$ m). However, the distributions of small and large particles at this cross section differ due to radial segregation, Figs. 2(b) and 2(c). Small particles are deep in the flowing layer and in the nonflowing core while large particles are near the surface and in the nonflowing periphery near the tumbler wall. As a result, in the flowing layer the axial flux of small particles away from the end wall in the upstream portion ($q_s < 0$) is larger than the flux toward the

end wall in the downstream portion ($q_s > 0$), Fig. 2(d). Thus, small particles are conveyed away from the end wall. The opposite is true for large particles, Fig. 2(e). The axial flux of large particles away from the end wall in the upstream portion ($q_l < 0$) is less than axial flux of large particles toward the end wall ($q_l > 0$) in the downstream portion. Thus, in the upstream portion of the flowing layer where the particles are mixed, both small and large particles move away from the end wall. Because of radial segregation, small particles percolate to the lower part of the flowing layer where the axial velocity back toward the end wall is less, while the large particles in the top of the layer are in a region of higher axial velocity back toward the end wall. The net result is that small particles carried away from the end wall in the upstream portion of the flowing layer are less likely to return to near the end wall in the downstream portion, whereas large particles carried away from the end wall in the upstream portion are more likely to return in the downstream portion resulting in steadily increasing degree of segregation.

The role of the end walls in axial band formation becomes clearer by simulating the same system with frictionless end walls. In this case, no significant axial flow occurs and no bands form. Likewise, using periodic boundary conditions also eliminates axial flow at the end walls. At the same rotation rate, $\omega = 3.14$ rad/s, the magnitude of the concentration fluctuations remains very small and no segregation bands appear in the system after 200 rotations. When the rotational speed is increased to $\omega = 6.28$ rad/s, some local extrema of concentration gradually evolve into segregation bands, as shown in Fig. 3. Consistent with the results with end walls, the band of large particles has a slightly larger angle of repose than the band of small particles, and axial flow occurs between segregation bands, though the axial velocities are lower than with end walls. The dependence of axial segregation on the rotational speed is consistent with experiments [5] where bands form only at higher rotational speeds and initially segregated bands tend to resolve to a mixed state at lower speeds. Not all concentration fluctuations develop into bands, and the final segregation bands originate from a subset of the early concentration fluctuations. Cross-sectional slices at $z = -0.03$ and 0.055 m are similar to those in Fig. 2 in that the radial segregation of particles
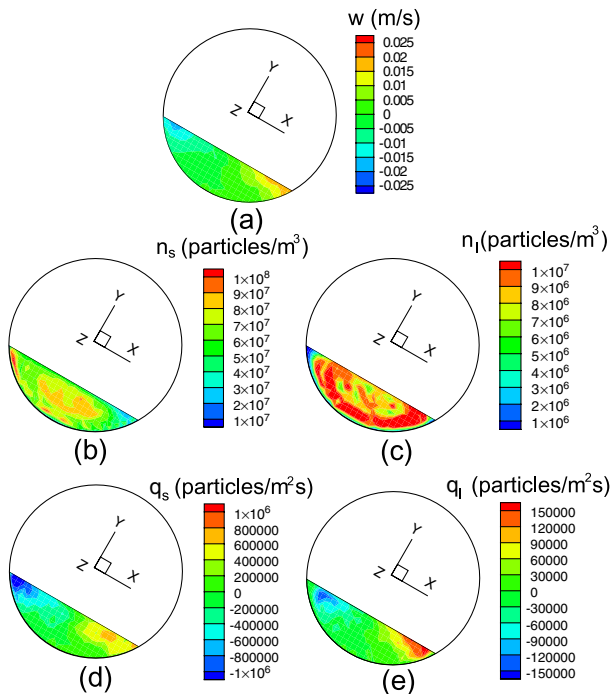

FIG. 2 (color online). Illustration of imbalanced distribution of the axial flow rate of particles in the cross section at $z = 0.065$ m averaged over rotation 0–1. (a) Axial velocity field of the mixture, (b) number density of small particles, (c) number density of large particles, (d) axial flux of small particles, (e) axial flux of large particles.
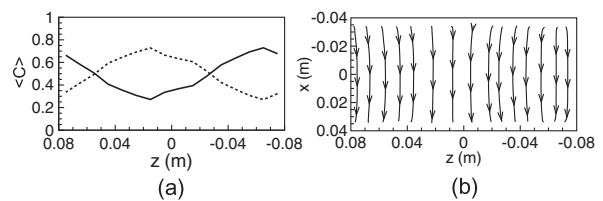

FIG. 3. (a) Cross-sectionally averaged species concentrations (dashed line, concentration of small particles; solid line, concentration of large particles), and (b) the velocity field on the free surface at $y = -0.02$ m along the axial length for periodic boundary conditions with $\omega = 6.28$ rad/s after 50 rotations.
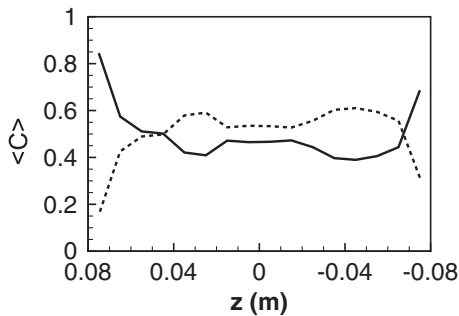
FIG. 4. Cross-sectionally averaged species concentrations (solid line, light particles; dashed line, dense particles) for a density system with $\omega = 6.28$ rad/s after 100 rotations.

results in small and large particles being in different regions of the downstream axial flow causing the particles to segregate into bands.

These findings depart from the conventional mechanism assumed for axial segregation. Although different angles of repose for segregated bands occur, axial flow drives the segregation. The nonuniform distributions of axial velocity and species concentrations on the cross section introduce an unbalanced distribution of axial flow of individual species in the upstream and downstream portions: small and large particles flow away from the end wall (or center of a large-particle band) in the upstream portion, but more large particles flow back toward the end wall (or center of a large-particle band) in the downstream portion because radial segregation has carried small particles deeper into the flowing layer where the axial velocity is smaller. This differential transport of small and large particles in a cross-sectional slice has been represented as a ''negative'' diffusivity in *ad hoc* models for axial segregation [4–6,12,26,27], even though this is clearly not a diffusion process.

This mechanism also explains experiments for density systems of same-size heavy and light particles [28–31], in which light particles accumulate at the end walls but no bands form, as shown in Fig. 4 for simulations with equal volumes of 2 mm diameter particles with $\rho = 2500$ and 7500 kg/m^3. In this case, radial segregation occurs throughout the tumbler, but axial flow only occurs near the end walls. Both particle types flow away from the end walls in the upstream portion of the flowing layer. In the downstream portion heavy particles fall deeper into the flowing layer where the axial flow is smaller, while light particles near the surface flow back toward the end walls to concentrate there. Why bands do not form away from the end walls in density systems (both experiments and simulations) is yet to be explained. Another open issue is the origin of the spontaneous bands in Fig. 3 that are unrelated to end walls. These likely arise from random concentration perturbations, but this is yet to be proven.

*r-lueptow@northwestern.edu

[1] Y. Oyama, Sci. Pap. Inst. Phys. Chem. Res. **37**, 17 (1940).
[2] M. B. Donald and B. Roseman, Br. Chem. Eng. **7**, 749 (1962).
[3] M. Nakagawa, Chem. Eng. Sci. **49**, 2540 (1994).
[4] O. Zik, D. Levine, S. G. Lipson, S. Shtrikman, and J. Stavans, Phys. Rev. Lett. **73**, 644 (1994).
[5] K. M. Hill and J. Kakalios, Phys. Rev. E **49**, R3610 (1994).
[6] K. M. Hill and J. Kakalios, Phys. Rev. E **52**, 4393 (1995).
[7] N. Jain, D. V. Khakhar, R. M. Lueptow, and J. M. Ottino, Phys. Rev. Lett. **86**, 3771 (2001).
[8] D. Gupta, D. V. Khakhar, and S. K. Bhatia, Chem. Eng. Sci. **46**, 1513 (1991).
[9] S. J. Fiedor and J. M. Ottino, Phys. Rev. Lett. **91**, 244301 (2003).
[10] T. Arndt, T. Siegmann-Hegerfeld, S. J. Fiedor, J. M. Ottino, and R. M. Lueptow, Phys. Rev. E **71**, 011306 (2005).
[11] G. Juarez, J. M. Ottino, and R. M. Lueptow, Phys. Rev. E **78**, 031306 (2008).
[12] S. B. Savage, in *Disorder and Granular Media*, edited by D. Bideau and A. Hansen (Elsevier Science, Amsterdam, 1993), pp. 255–285.
[13] Z. S. Khan, W. A. Tokaruk, and S. W. Morris, Europhys. Lett. **66**, 212 (2004).
[14] K. M. Hill, A. Caprihan, and J. Kakalios, Phys. Rev. Lett. **78**, 50 (1997).
[15] P. A. Cundall and D. L. Stack, Geotechnique **29**, 47 (1979).
[16] G. H. Ristow, *Pattern Formation in Granular Materials* (Springer, New York, 2000).
[17] J. Schafer, S. Dippel, and D. E. Wolf, J. Phys. I (France) **6**, 5 (1996).
[18] P. Chen, J. M. Ottino, and R. M. Lueptow, Phys. Rev. E **78**, 021303 (2008).
[19] D. C. Rapaport, Phys. Rev. E **65**, 061306 (2002).
[20] N. Taberlet, M. Newey, P. Richard, and W. Losert, J. Stat. Mech. (2006) P07013.
[21] D. C. Rapaport, Phys. Rev. E **75**, 031301 (2007).
[22] P. Chen, B. J. Lochman, J. M. Ottino, and R. M. Lueptow, Phys. Rev. Lett. **102**, 148001 (2009).
[23] L. E. Silbert, G. S. Grest, R. Brewster, and A. Levine, Phys. Rev. Lett. **99**, 068002 (2007).
[24] C. S. Campbell, J. Fluid Mech. **465**, 261 (2002).
[25] N. A. Pohlman, J. M. Ottino, and R. M. Lueptow, Phys. Rev. E **74**, 031305 (2006).
[26] I. S. Aranson and L. S. Tsimring, Phys. Rev. Lett. **82**, 4643 (1999).
[27] I. S. Aranson, L. S. Tsimring, and V. M. Vinokur, Phys. Rev. E **60**, 1975 (1999).
[28] L. Sanfratello and E. Fukushima, Granular Matter **11**, 73 (2009).
[29] S. Ahmed, S. E. John, I. D. Sutalo, G. Metcalfe, and K. Liffman (to be published).
[30] D. Hayter, G. Pereira, K. Liffman, B. Aldham, S. Johns, I. D. Sutalo, G. Brooks, P. Cleary, and G. Metcalfe, Proc. SPIE Int. Soc. Opt. Eng. **7270**, 727010 (2008).
[31] G. G. Pereira, M. D. Sinnott, P. W. Cleary, K. Liffman, G. Metcalfe, and I. D. Sutalo (to be published).